Wet electrospinning of poly(butylene succinate)(PBS) copolyester into helically coiled 3D structures

*Agueda Sonseca[†], Rahul Sahay[†], Karolina Stepien[†], Aleksandra Wcislek[†], Andrew McClain[§], Peter Sobolewski[†], XiaoMeng Sui[£], Judit E. Puskas[§], H. Daniel Wagner[£], Joachim Kohn[ξ], Miroslawa El Fray[†]**

[†] West Pomeranian University of Technology, Szczecin, Polymer Institute, Functional Materials and Biomaterials, Faculty of Chemical Technology and Engineering, Al. Piastow 45, 71-310 Szczecin, Poland

[§] The University of Akron, Akron Engineering Research Center AERC, Akron, OH, USA

[£] Department of Materials and Interfaces, Weizmann Institute of Science, Rehovot, 76100, Israel

[ξ] New Jersey Center for Biomaterials, Rutgers, The State University of New Jersey, Piscataway, NJ, USA

*Corresponding author: mirfray@zut.edu.pl

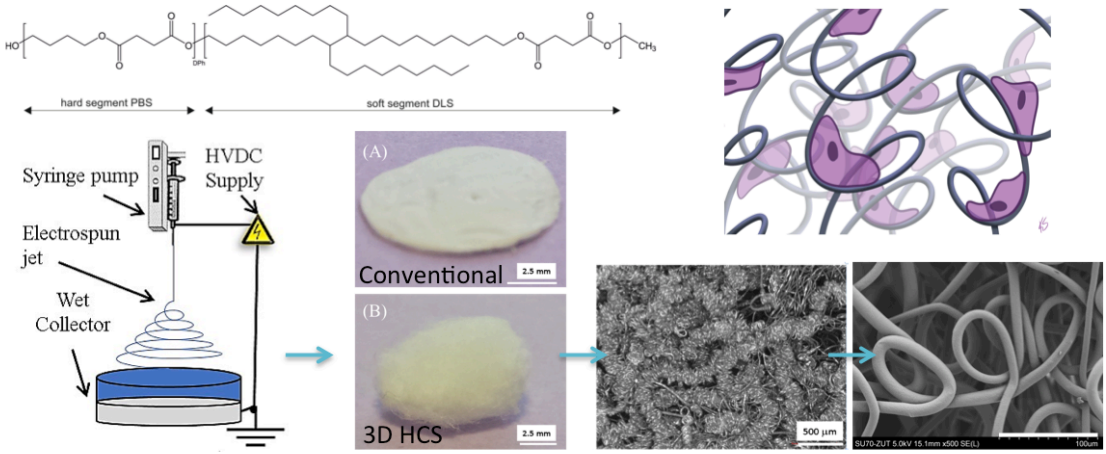

ABSTRACT: Electrospinning is one of the most investigated methods used to produce polymeric fiber structures that mimic the fiber morphology of native extracellular matrix. These structures have been extensively studied in the context of scaffolds for tissue regeneration. However, the compactness of materials obtained by traditional electrospinning, collected as two-dimensional non-woven membranes, can limit cell infiltration and tissue ingrowth. In addition, for applications in smooth muscle tissue engineering, highly elastic scaffolds capable of withstanding cyclic mechanical strains without suffering significant permanent deformations are preferred. In order to address these challenges, we report the fabrication of microscale 3D helically coiled structures (referred as 3D-HCS) by wet-electrospinning method, a modification of the traditional electrospinning process in which a coagulation bath (non-solvent system for the electrospun material) is used as the collector. The present study successfully demonstrates the feasibility of using this method to process segmented copolyester poly(butylene succinate-co-dilinoleic succinate) (PBS-DLS), a thermoplastic elastomer, into 3D helically coiled structures (HCS). A mechanism for the HCS formation is proposed and verified with experimental data. Fabricated 3D-HCS showed high specific surface area, high porosity, and good elasticity. Further, the marked increase in cell proliferation on 3D-HCS confirmed the suitability of these materials as scaffolds for soft tissue engineering.

KEYWORDS: electrospinning; polyester; scaffolds; coagulation bath; helically coiled fibers

INTRODUCTION

Natural materials are characterized by their complex hierarchal structures with a tight coupling between structure and function. These aspects have served as inspiration for materials scientists and engineers in the design of advanced functional materials.[1] Of particular interest are micro/nanoscale helically coiled structures (HCS), possessing unique morphology and interesting properties (electrical, magnetic, optical, etc.) as well as high stretchability and mechanical stability.[2,3] The techniques employed to fabricate nanoscale helical structures include sol-gel, selective etching, and self-organization.[4–6] For example, manganese oxide helical structures have been produced from the contraction of a sol-gel in a capillary tube upon solvent evaporation,[5] while Kong *et al.*[7] obtained zinc oxide nano-helical structures by induced spontaneous polarization.

Varied fiber morphologies, including HCS, can also be obtained by electrospinning.[8] Different strategies have been reported to achieve the microscale coiled morphology, based either on the combination of two polymers with specific different physical properties, like differential shrinkage or conductivity,[9–11] or in single polymeric systems, by modifying the concentration of the polymer and/or the solvent system.[12,13] While various applications of these materials can be envisioned, some of the properties of such coiled electrospun fiber structures, such as high porosity, flexibility and elasticity, are particularly advantageous in the context of tissue engineering scaffolds or templates. Further, the past 20 years have seen a shift to so-called "functional tissue engineering," which emphasizes the critical role of structure and biomechanics in tissue engineering functional tissue constructs.[14,15] In this context, HCS mimic the architecture and behavior of human soft tissues, such as the heart muscle perimysium composed of microscale coiled fibers.[16] Additionally, highly elastic scaffolds based on elastic biomaterials have been demonstrated to better maintain their integrity (low permanent deformations) and structure,[17,18] which is especially useful when working under cyclic loads, such as occurs in cardiac muscle. However, all these traditional

electrospinning based methodologies have yielded 2D coiled structures, while functional tissue constructs need to be 3D. Highly porous, 3D structures can be obtained via an alternative electrospinning approach: using a coagulation bath of non-solvent as the collector.[19–30] While these studies produced 3D structures composed of fibers that are not straight, the random fiber morphology is very far from the desired coiled, hierarchal morphology. However, recent work by Taskin *et al.*[31] describes electrospinning polycaprolactone (PCL) into an ethanol coagulation bath to obtain highly porous 3D structures composed of coiled fibers, which facilitated myofibroblast differentiation and contraction. While these results are very promising, PCL is a thermoplastic polyester and lacks the elastomeric properties crucial for truly functional cardiac tissue engineering.

Here we demonstrate the effectiveness of wet-electrospinning for the fabrication of microscale 3D HCS from a new segmented copolymer, namely poly(butylene succinate-co-dilinoleic succinate)(PBS-DLS). Our goal was to mimic both the 3D coiled morphology and the elasticity of the perimysium of cardiac tissue. The PBS-DLS 70:30 copolymer chosen for template fabrication belongs to the family of polyester thermoplastic elastomers, based on succinic acid, 1,4-butanediol and dilinoleic diol, that we have developed for heart tissue engineering.[32] PBS-based copolymers containing dilinoleic acid/diol degrade into non-cytotoxic products and their properties can be modulated by varying the ratio of hard to soft segments covering a wide range of strength and elasticity.[32–35] Therefore, PBS-DLS represents a good candidate material to contribute elastic properties to the scaffold, in synergy with the 3D HCS morphology. We investigated the morphology, thermal, and mechanical properties of 3D HCS, as well as their cytocompatibility. Furthermore, we elaborate a critical analysis of the forces acting on the electrospun jet in order to understand the evolution of HCS morphology during wet-electrospinning.

MATERIALS AND METHODS

Dichloromethane (DCM: ⩾99.5%), succinic acid (SA: ⩾99%) and 1,4-butanediol (BD: 99%) were purchased from Sigma Aldrich (Poznań, Poland). Dimer linoleic diol (named here as dilinoleic diol), (DLA–OH) Pripol™ 2033 (dimer alcohol ⩾96.5%), was purchased from Croda Coatings & Polymers, Gouda (The Netherlands). Chloroform ($CHCl_3$: ⩾98.5%) and methanol (MeOH: ⩾99.8%) were purchased from POCh (Gliwice, Poland) and titanium dioxide based catalyst, $(TiO)_2$ (C-94, Huntsman). All the reagents were used as received.

Synthesis of PBS-DLS copolymer

Poly(butylene succinate-co-dilinoleic succinate) 70:30 wt.% of hard to soft segments was synthesized as part of a multiblock copolymers series containing dimer linoleic diol. DLA-OH was employed as building block of the dilinoleic-succinate soft segments (DLS) while poly(butylene succinate) (PBS) units conformed the hard segments (Figure 1). Previously reported two-step synthesis procedure for PBS-DLS 50:50 copolymer was employed.[33] Briefly, esterification stage (1st step) was carried out at 180 ºC, until 95% of theoretical amount of water sub-product was collected, in the presence of succinic acid, 1,4-butanediol and titanium dioxide based catalyst $(TiO)_2$ (C-94). Dilinoleic diol was added to the reaction mixture, temperature was increased to 250 ºC at an approximated rate of 1.5 ºC/min, and pressure was decreased to 0.2 - 0.4 hPa in order to start the polycondensation stage (2nd step). The reaction was monitored by power consumption of the stirrer and was finished when indicated that the highest melt viscosity was reached. The molar ratio between acid and diols was set at 1:2.2.

Electrospinning process

The electrospinning setup consisted of high voltage direct current power supply (Gamma HV Research ES30P) attached to the 21 G needle. Polymer solution was fed through the needle via a syringe inserted in a syringe pump (Ascor AP14). The counter-electrode was either a

conventional grounded metallic flat collector (length ~15 cm and width ~15 cm) or a non-solvent coagulation bath (see **Figure 1**). The non-solvent bath was a shallow glass container with diameter ~19.5 cm and height ~2 cm. Electrospinning was performed at ~25 °C temperature and ~30% relative humidity. Various parameters of both conventional and bath collector processes were varied in order to study and optimize the fiber morphology and thereby template characteristics, including copolymer solution concentration, system parameters (voltage, distance), and different non-solvent coagulation baths (deionized water or methanol). After both conventional and wet electrospinning, membranes were vacuum dried for 72 h and morphology was characterized using laser scanning microscopy (LSM, Keyence VK-9700K) and scanning electron microscopy (SEM, Hitachi SU-70). Samples for LSM were visualized without any preparation, while samples for SEM were sputtered with a 60 Å layer of gold.

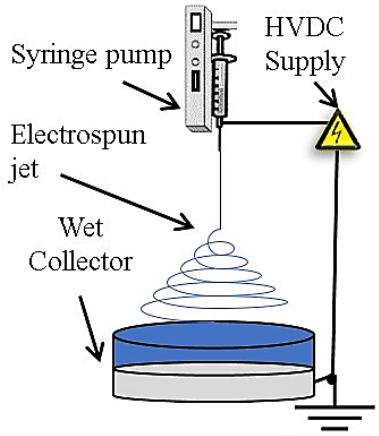

Figure 1. Schematic of wet-electrospinning setup used for collecting helically coiled structures.

Characterization Methods

The chemical structure of the obtained copolymer was verified by nuclear magnetic resonance (^{1}H NMR, ^{13}C NMR) and infrared spectroscopy (ATR-FTIR). TM Bruker DPX 400 (400 MHz) spectrometer was used to record ^{1}H NMR (128 scans, 1 second relaxation delay) and ^{13}C NMR (5120 scans, 1 second relaxation delay) spectra. $CDCl_3$ was employed as

a solvent and tetramethylsilane (TMS) as an internal reference. FTIR transmission spectra were collected and averaged from 32 scans across the spectral range of 400 to 4000 cm^{-1}, with a 2 cm^{-1} resolution, using a Bruker ALPHA spectrometer with an Attenuated Total Reflectance (ATR) cell. Samples were vacuum-dried prior to measurement.

The number-average molecular weight (M_n), weight-average molecular weight (M_w), and polydispersity index (PDI) of the PBS-DLS copolymer were determined by gel permeation chromatography (GPC). The experiment was conducted on a Tosoh EcoSEC, equipped with 2 fused silica separation columns and four detection systems: Dual Absorbance UV (UV, Waters 2487, wavelength λ =254 nm), multi-angle laser light scattering (MALLS, Wyatt mini-DAWN Treos), refractive index (RI, Wyatt OPTILAB DSP), and viscometer (VIS, Wyatt ViscoStar-II). The results were analysed using ASTRA 6 software (Wyatt Technology). The sample concentration was 2-3 mg/mL and $CHCl_3$ (HPLC grade, Alfa Aesar), continuously distilled from CaH_2, was used as eluent at a flow rate of 0.7 mL/min; the injected volume was 15 µl. The runtime was 60 min, in order to avoid the aftereffect of the viscometer in the differential refractive index (dRI) signal. The incremental refractive index (*dn*/*dc*) was calculated from the concentration and calculated mass, assuming 100% mass recovery from the columns.

The thermal behaviour of PBS-DLS 70:30 was studied using a TA Instruments DSC Q100 differential scanning calorimeter. Measurements were carried out in a heating–cooling–heating cycle over the temperature range from -90 to 200 ºC, at a heating/cooling rate of 10 °C min^{-1}, under a N_2 atmosphere. The glass transition temperature (T_g) was calculated as the midpoint of the transition in the second heating run.

The mechanical characterization of electrospun samples was performed by static tensile testing, using a universal testing machine (Instron 3366, Instron Co., Ltd., USA) at room temperature. The measurements were carried out at the crosshead speed of 1 mm/min from 0 to 0.5% elongation (to calculate the Young's modulus) and 10 mm/min from 0.5%

elongation using a 500 N load cell. In order to handle easily the electrospun materials and avoid preloads on the samples before the mechanical tests, square paper frames were used. The samples were cut into rectangular strips, 5 mm wide and 4 cm long, while the internal length of the framework was 2 cm. Sample thickness was measured by using a coating thickness gauge (Elcometer Instruments GmbH, Germany) with Elcometer thickness standards, before the test.

The porosity of samples was measured using liquid displacement method with ethanol as the immersing liquid (ρ= 0.80424 g/cm^3) at 19 °C. The, open porosity, P_0 (Equation 1), was calculated as follows:

$$P_0 = \frac{(m_n - m_s)}{(m_n - m_w)} \cdot 100\% \quad (2)$$

Where, P_0 is the open porosity, m_s is the mass of dry sample [g], m_n is the mass of sample saturated by immersion liquid [g], m_w is the mass submerged in the immersion liquid [g].

In vitro cell culture

Cytotoxity of electrospun membranes was tested via extract test and direct contact test, based on ISO10993-5,[36] using L929 murine fibroblasts. Briefly, sub-confluent (70-80%) T25 flasks were trypsinized, cells were counted, and 10,000 cells were plated per well of a 96 well plate in 100 µL of complete media (DMEM containing 10% fetal bovine serum (FBS), 2 mM L-glutamine, 100 U/mL penicillin, and 100 µg/mL streptomycin). After 24 hours of culture, cells were either exposed to extracts or samples of electrospun fiber membranes.

For extracts, conventionally electrospun PBS-DLS membranes (50-100 µm thick) were cut into 0.5 cm^2 strips and disinfected by soaking in 70% isopropyl alcohol for 20 minutes. Samples were then triple rinsed in sterile PBS, placed into tubes containing 0.5 mL of complete cell culture media, and incubated at 37 °C for 24 hours (a tube containing just media was used as a vehicle control). After incubation, media was collected and (neat or diluted 1:3 with fresh media) used to replace the media of L929 cells seeded 24 hours in advance. After

further 24 hours of culture, viability of cells was assessed using resazurin assay.[37] Briefly, 0.15 mg/mL sterile resazurin stock in PBS was diluted 1:6 with complete media and 100 μL was added to each test well after aspirating media. Plate was then incubated for 4 hours at 37 °C and fluorescence (Em: 540, Ex: 590) was measured using BioTek Synergy HTX multifunctional plate reader.

For direct contact tests, 4 mm diameter discs of conventionally electrospun PBS-DLS membranes were cut using pneumatic punch, disinfected by soaking in 70% isopropyl alcohol for 20 minutes, and triple rinsed in sterile PBS. Samples were then placed on top of L929 cells seeded 24 hours in advance (following aspiration of media), held in place using Scaffdex CellCrown 96 insert, and covered with 140 μL of complete media. As a control, inserts were placed into wells without samples. After 48 hours of culture, inserts and materials were removed and cell viability was assessed using resazurin assay as described above.

In order to compare cell response to conventionally electrospun 2D membranes and HCS, 4 mm diameter samples of conventionally electrospun membranes and HCS were cut using pneumatic punch, disinfected by soaking in 70% isopropyl alcohol for 20 minutes, triple rinsed in sterile PBS, and rinsed in complete media. Each sample was then loaded into a Scaffdex CellCrown 96 insert and the inserts were placed into 96 well-plate wells containing 75 μL of complete media. Next, 20,000 L929 cells in 25 μL of complete media were carefully pipetted on top of each sample, within the CellCrown 96 insert. After 18 hours of culture to allow for adhesion of cells, inserts were transferred to empty wells and the resazurin assay was used to assess viability as described above. Cells were then maintained in culture on membranes and viability was assessed again after additional period of 48 hours (66 total) and then an additional period of 96 hours (162 hours total). Data was analysed using R software. Comparisons were tested by first F-testing for equality of variances, followed by two-sample t-test.

RESULTS AND DISCUSSION

Fabrication of 3D HCS. PBS-DLS copolymer containing 70:30 wt% of hard to soft segments ratio (**Figure 2**) was synthesized by melt polycondensation and its chemical structure was analysed by ^{1}H NMR (Supporting information, Figure SI.1). IR spectrum of segmented copolymer revealed bands characteristic for polyester and their detailed assignments are given in Supporting information (Figure SI.2). Table 1 summarizes PBS-DLS chemical and physical properties.

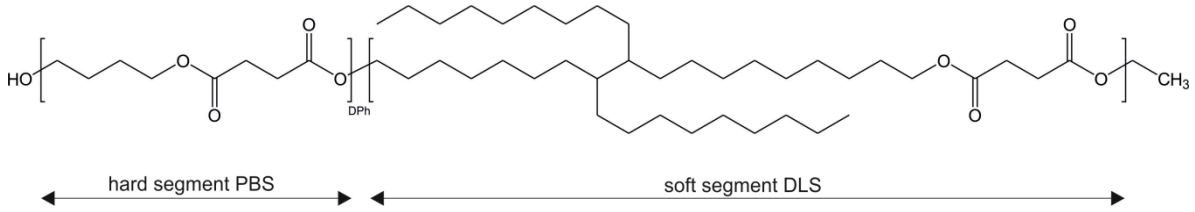

Figure 2. Chemical structure of poly(butylene succinate-co-dilinoleic succinate) PBS:DLS 70:30 copolymer. DPh – degree of polycondensation of hard segments, 8.49.

Table 1. Chemical and physical properties of PBS-DLS copolymer

Sample	$^{a}M_w$ (10^3 g mol^{-1})	$^{a}M_n$ (10^3 g mol^{-1})	$^{a}M_w/M_n$	$^{b}T_c$ (°C)	$^{b}T_g$ (°C)	$^{b}T_m$ (°C)	^{b}Xc (%)
PBS-DLS 70:30	62.3	23.8	2.6	48.3	-44.4	98.7	28.7

[a] calculated from GPC/SEC, [b] based on DSC
M_w – weight average molar mass, M_n – number average molar mass; M_w/M_n – dispersity index, T_c – crystallization temperature, T_g – glass transition temperature, T_m – melting point of hard segments, X_c – degree of crystallinity of hard segments.

In order to achieve uniform, dense 3D HCS, the parameters of the wet-electrospinning process were varied. These parameters included concentration of polymer solution, applied electric field (voltage, distance), and flow rate of the polymer solution. The concentration of the PBS-DLS 70:30 in chloroform was varied from 15 to 35 wt/v%. For a given applied electric field

and flow rate, concentrations below 20 wt/v% resulted in bead-on-string structures, whereas above and including 20 wt/v% resulted in uniform HCS.

The effect of the non-solvent coagulation bath was also tested, by comparing deionized water, ethanol, and methanol. When water was used, random electrospun fibers were collected as shown in **Figure 3a**. This is attributed to hydrophobic nature of PBS-DLS fibers, which float on the surface of water (γ = 72.86 mN/m) forming an nonwoven fibrous network. On the other hand, uniform HCS were collected when methanol was used for the coagulation bath (see **Figure 3b**). In this case, electrospun fibers also collect on the surface of the non-solvent bath, but later sink, creating 3D HCS in the bulk of the liquid bath[19,20,23,28]. In addition to methanol, we also tested ethanol as non-solvent. No major differences were observed in the morphology of the HCS obtained in either alcohol bath, likely due similar surface tensions of methanol (γ = 22.50 mN/m) and ethanol (γ = 22.10 mN/m). As a result, for the remainder of the experiments presented, only HCS collected in methanol bath are discussed.

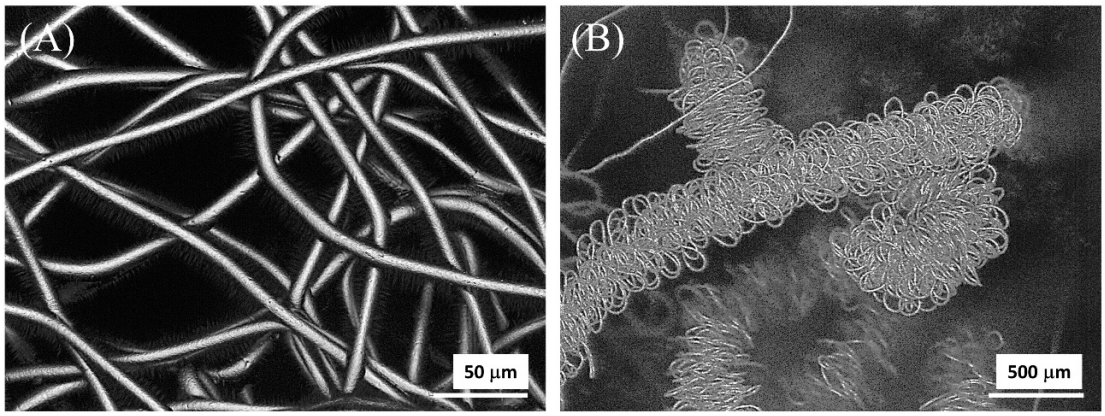

Figure 3. LSM images of 30 w/v% PBS:DLS 70:30/$CHCl_3$ collected on (a) water bath as 2D electrospun membrane at flow rate ~10 ml/h and electric field ~0.7 KV/cm, (b) methanol bath as 3D electrospun HCS at flow rate ~10 ml/h and electric field ~0.58 KV/cm.

Figure 4 shows macroscopic and LSM images of PBS-DLS 70:30 electrospun membranes obtained by conventional electrospinning (Figure 4A) and wet electrospinning

system filled with MeOH as a non-solvent in the coagulation bath (Figure 4B). As expected, conventional electrospinning yields dense 2D non-woven membranes of PBS-DLS. However, using the non-solvent methanol bath as the collector favors the formation of 3D fibrous HCS.

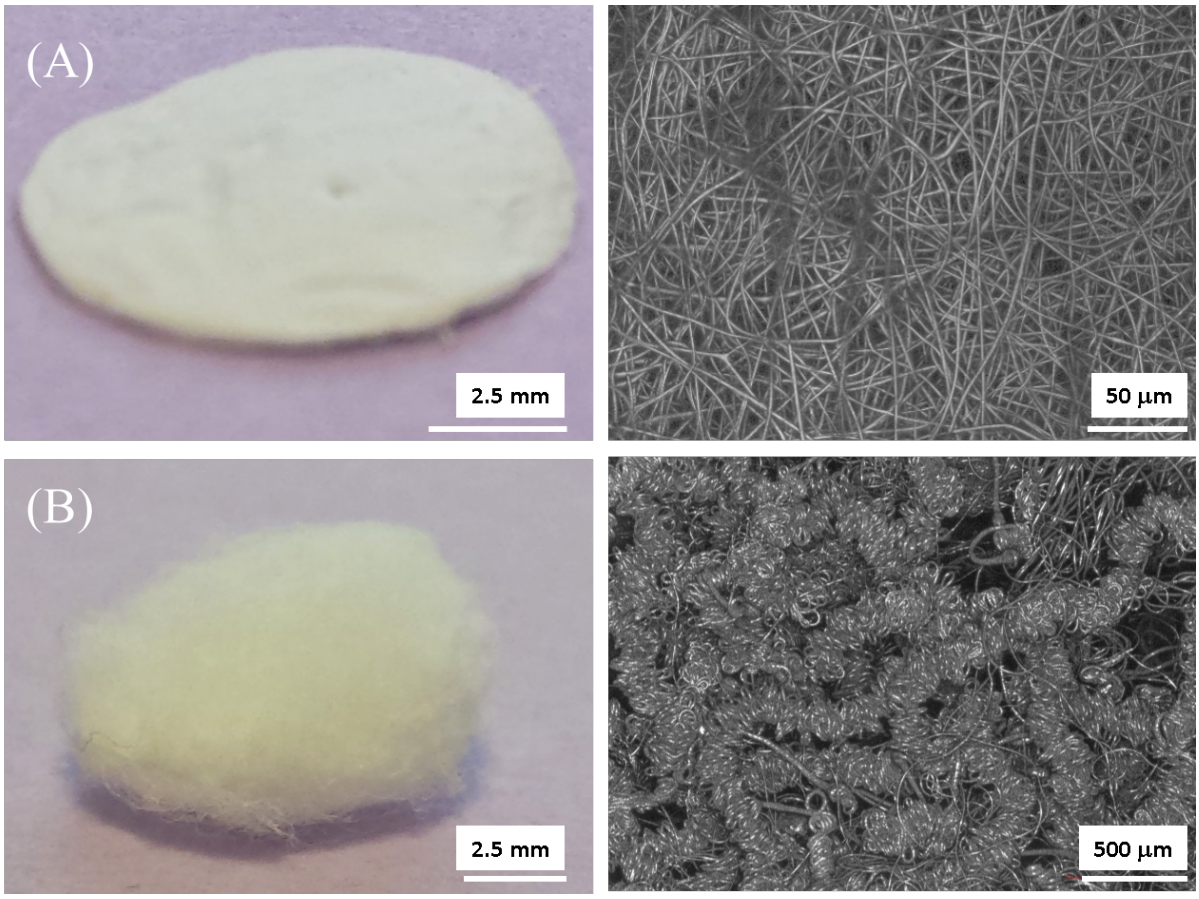

Figure 4. Electrospun membranes collected on (a) conventional flat collector covered with aluminum foil for 16 wt/v% PBS:DLS 70:30 in $CHCl_3$: MeOH (7:3) as a solvent electrospun at electric field ~1 kV/cm, and flow rate ~6 ml/hr as 2D membrane, and (b) methanol bath for 20 wt/v% PBS:DLS 70:30 in $CHCl_3$ electrospun at electric field ~0.65 kV/cm, and flow rate ~7 ml/hr as 3D membrane consisting of HCS.

Thanks to the low surface tension of MeOH (γ = 22.50 mN/m), during wet electrospinning the fibers sink into the coagulation bath and the liquid prevents subsequent fibers from piling up, favouring a loosely packed structure. The morphology of our PBS-DLS HCS is similar to that of 3D scaffolds obtained from PCL by Taskin *et al.,*[31] however we observe that the individual coils are more dense and spring-like. Overall, it was possible to obtain varied HCS

morphologies and utilize different polymer-solvent systems, such as 20 w/v% PBS-DLS (70:30)/dichloromethane solution (**Figure 5**), thus the process can be adapted to various applications in functional tissue engineering and beyond.

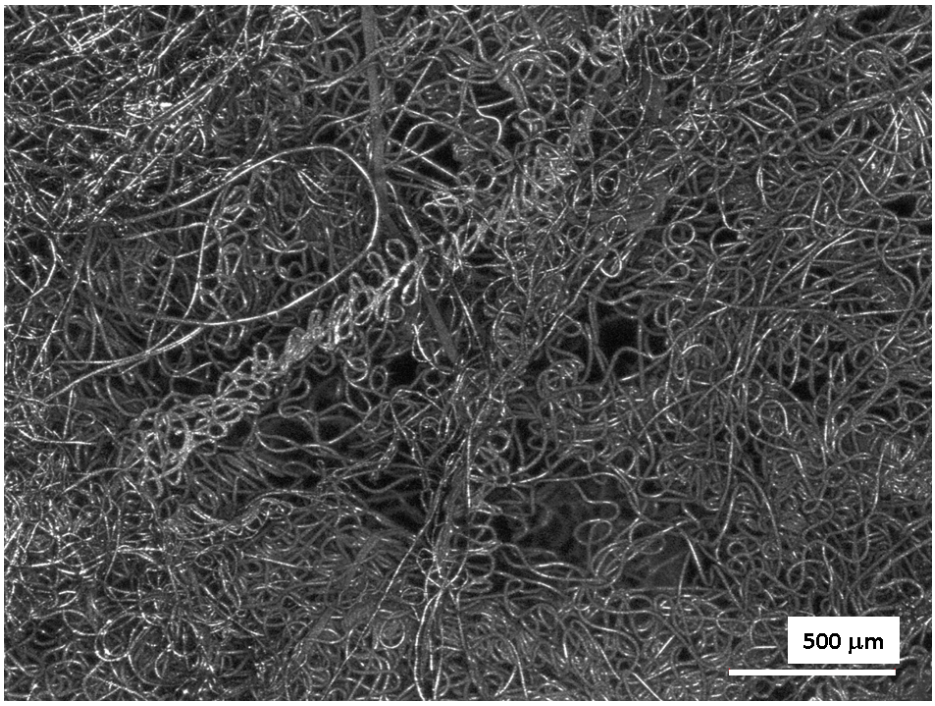

Figure 5. LSM images of 3D electrospun membrane from 20 wt/v% PBS:DLS 70:30/ dichloromethane solution collected in a methanol bath electrospun at electric field ~0.54 kV/cm, and flow rate ~10 ml/hr.

In order to understand the process of coil formation and resulting HCS morphology, we examined the governing mechanics. Over the years, researchers have proposed various mechanisms for the production of HCS. Typically, HCS are formed by twisting of the fiber under the action of tensile force. Ross *et al.* [38,39] defined the critical torque (τ_c) that initiates coiling in anisotropic fibers under a tensile force (F_t) as:

$$\tau_c = \sqrt{2F_t EI} \qquad (2)$$

where, E is the fiber's Young's modulus and I is its second moment of area ($\pi d^4/64$), considering that the fiber has a circular cross-section with diameter d. Thus, the expression of critical torque for electrospun jet can be rewritten as follows:

$$\tau_c = \sqrt{(F_t - F_v)\frac{E\pi d^4}{32}} \quad (3)$$

where the tensile force due to the electrical force acting on the jet can be defined as $F_t \approx \sigma A_t E_e$, σ being the surface charge density of electrospun jet, A_t the cross-sectional area of the jet and E_e the applied electric field.[40] F_v is the viscoelastic restoring force, inhibiting stretching of the jet during electrospinning.

As expected, either twisting or bending can provide the torque required to coil the fiber. In case of electrospinning, the electrospun jet after a straight-line motion suffers from bending instabilities leading to non-uniform helical motion of the jet.[41] The torque required for this helical motion of the electrospun jet is provided by normal electric, given by formula (4):

$$F_n \approx \frac{(\bar{\varepsilon}-\varepsilon)}{2} A_n {E_e}^2 \quad (4)$$

where, $\bar{\varepsilon}$ and ε are the dielectric constant of the surrounding fluid and jet, respectively, and A_n is the surface area of the jet.[40]

Therefore, it is inferred that similar to non-uniform helical motion experienced by electrospun jet, F_n is also critical for the formation of HCS. Reduction in F_t or an increase in F_v will reduce the torque required to initiate coiling, but F_n will provide the actual torque for HCS formation (see Eq. 5). The viscoelastic force (F_v) act as restoring force resisting the stretching and bending of the electrospun jet *i.e.* it acts against both F_t and F_n. Apart from F_n, differential viscoelastic stretching as observed for bicomponent fiber system, can also lead to bending of the electrospun jet and formation of coiled structures.[10]

Further, HCS were only collected in liquid non-solvent coagulation bath; therefore, it is important to consider the forces acting on electrospun jet when it comes in contact with the

liquid in coagulation bath (Table 2). Typically, when a micro/nanoscale elastic/viscoelastic structure contacts a liquid interface, capillary forces can be strong enough to induce bending or wrinkling in such structures.[42–44] Thus, when using a coagulation bath, the surface tension force (F_s) of the liquid will also contribute to the bending of the electrospun jet and to HCS fabrication.

Therefore, the electrospun jet will be under the influence of F_t, F_n, F_s, and F_v during the formation of HCS in coagulation bath. Table 2 shows that F_t and F_n acting on electrospun jet are higher when collected on a coagulation bath than when collected on a metallic flat collector. F_v will oppose to the formation of HCS in both coagulation bath and on a flat collector, while F_s will promote the formation of HCS. In the absence of F_s *i.e.* conventional electrospinning, F_t and F_n were not sufficient enough to create HCS. Further, it was observed experimentally that in the absence of electric forces (F_t and F_n) *i.e.* in the absence of applied electric field, F_s is not sufficient enough to create HCS: the jet under the action of only gravitational force and F_s collected as polymeric globules at the bottom of coagulation bath.

Table 2. Comparison of forces experienced by electrospun jet collected onto flat collector in conventional electrospinning and coagulation bath in wet-electrospinning.

Parameters	Flat collector	Coagulation bath	Comparison
Normal electric force $F_n \approx \frac{(\bar{\varepsilon}-\varepsilon)}{2} A_n {E_e}^2$)	$\bar{\varepsilon} = 1; \varepsilon \sim 4.8;$ $(F_n)_{FC} \approx \frac{(-3.8)}{2} A_n {E_e}^2$	$\bar{\varepsilon} = 32.6; \varepsilon \sim 4.8;$ $(F_n)_{CB} \approx \frac{(-27.8)}{2} A_n {E_e}^2$	$\frac{(F_n)_{CB}}{(F_n)_{FC}} \approx 7.3$
Tensile electric force $(F_t \approx \sigma A_t E_e)$,	$\sigma \approx 0$, jet loses its charge as it comes in contact with metallic collector, therefore $(F_t)_{FC} \approx 0$	$\sigma \neq 0$ $(F_t)_{CB} \neq 0$	For a given time, charge diffusion from jet will be greater on metallic collector than on liquid bath $\frac{(F_t)_{CB}}{(F_t)_{FC}} > 1$

In our experimental studies, HCS were fabricated from different concentration of PBS-DLS 70:30 chloroform solutions (concentration above 20 wt/v%), therefore, F_v is not considered relevant for the fabrication of HCS in a liquid bath above a certain threshold concentration. Therefore, mainly F_t, F_n, and F_s are considered responsible for the formation of HCS in liquid bath. This described mechanism of formation of HCS in liquid bath can help future work aimed at obtaining HCS for a variety of applications.

Characterization of 3D HCS. 2D membranes, as well as 3D HCS were tested for their physical, as well as mechanical properties. SEM and LSM images were used to obtain average fiber diameter for both 2D membranes and 3D HCS (Table 3), as well as to compare their morphology (**Figure 6**). The analysis of coiled fiber morphology in 3D membranes indicated 9.9 μm average diameter, which is the same order of magnitude as collagen coiled fibers found in perimysium (diameter ~ 2 - 3 μm)[16]. Interestingly, as can be seen from SEM in Figure 6c, PBS-DLS HCS are composed of fibers that also have surface porosity (~250 nm), in contrast to fibers collected on aluminium foil (Figure 6a,b). The native biological environment of most cells is rich with topographical features in the 10-200 nm range and cells are known to respond to both defined topographies, as well as surface roughness.[45] We speculate that the surface porosity of PBS-DLS HCS may promote cell adhesion. Additionally, these pores could be further leveraged, for example, to facilitate controlled release of bioactive cues, such as growth factors, from within the polymer matrix.

a) b)

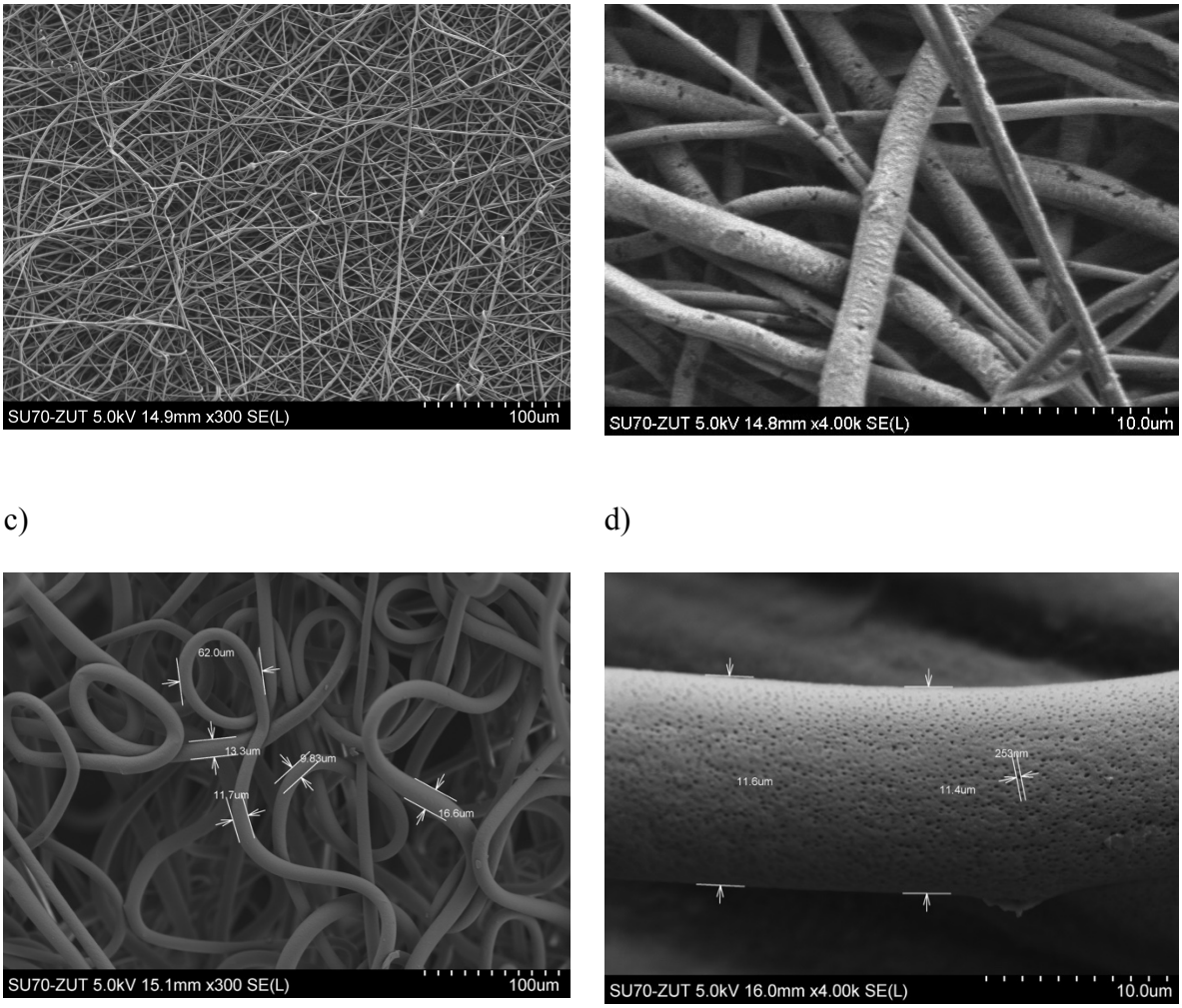

Figure 6. SEM images of electrospun templates from PBS-DLS 70:30/chloroform solution collected on (a,b) conventional flat collector covered with aluminium foil, and (c,d) methanol bath.

Porosity and apparent density of 2D membranes and 3D HCS were measured, as shown in Table 3. As expected, when compared with conventional electrospun 2D non-woven membranes, 3D HCS obtained by wet electrospinning show higher open (and apparent) porosities. This three-dimensional interconnected porosity of these 3D membranes should facilitate better cell distribution within the material and, thus, assembly of functional tissues. Collectively, the 3D HCS structure with high open porosity and surface nanoporosity should be well suited for cell seeding and ultimately heart tissue regeneration.

Table 3. Apparent density and porosity of traditional and wet electrospun membranes.

Sample	Conditions	V (kV)	Flow rate (mLh^{-1})	E (kV/cm)	d_{av} (μm)	C_{av} (μm)	Open porosity (%)
PBS-DLS 70:30, 20 wt/v% in $CHCl_3$	Methanol coagulation bath	15	10	0.65	9.87±2.35	370.83±50.17	85.4
PBS-DLS 70:30, 16 wt/v% in $CHCl_3$: MeOH (7:3)	Conventional electrospinning	17	6	1.0	0.86±0.30	-	76.1

V – voltage, E – electric field, d_{av} – average diameter of fiber, C_{av} – average coil diameter

Finally, we conducted mechanical tests to compare the tensile properties of 2D membranes with 3D HCS (**Figure 7**). For the 2D membranes, Young's modulus (E) was 11±0.45 MPa and tensile strength (σ) was 3.04±0.21 MPa. For the 3D HCS, the values are markedly lower: E=1.83±0.8 MPa and σ = 0.3±0.18 MPa. The lower values of E and σ of 3D HCS are attributed to its highly coiled and porous nature. Further, the mechanical properties of fabricated 3D membranes are a better match for the properties of cardiac tissue: E=0.2-0.5 MPa and σ = 3-15 kPa.[46] Therefore, we conclude that our membranes with the combination of elastomeric PBS-DLS and HCS morphology should be well suited to facilitate engineered cardiac tissue contractility.

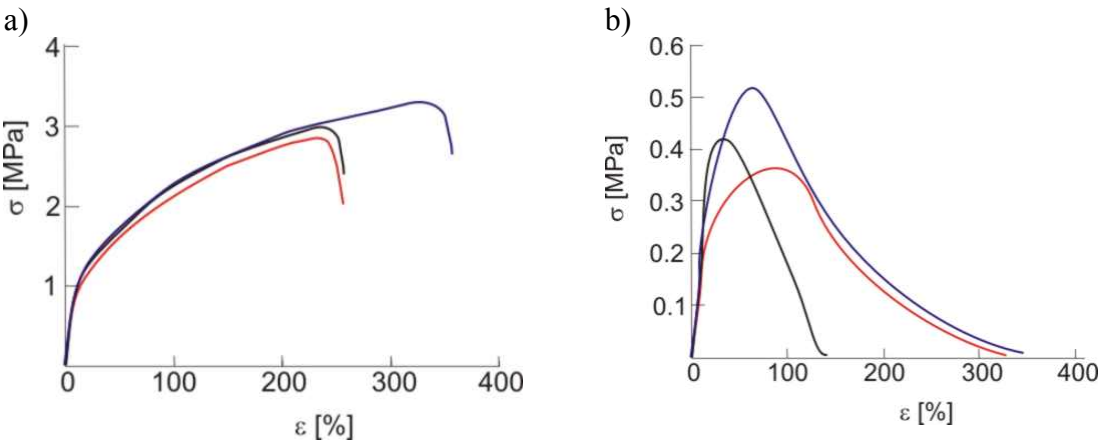

Figure 7. Stress-strain curves of (a) 2D electrospun PBS-DLS membranes, and (b) 3D HCS

Cytocompatiblity tests of 3D HCS. Cytocompatiblity tests were performed in order to confirm the potential of obtained HCS for functional tissue engineering. First, cytotoxicity assessment using extracts from conventionally electrospun 2D membranes (24 hours in complete media at 37 °C) indicated no cytotoxicity of electrospun PBS-DLS: cell viability of L929 murine fibroblasts after 24 hours exposure to undiluted extracts was 101±1% of vehicle control (n=3 samples, each extract was tested in triplicate). Likewise, following 48 hours of direct contact with samples, no growth inhibition zone was observed and resazurin viability test indicated 82±7% viability (n = 5 discs) of L929 cells in wells without discs, which is above the 70% threshold indicating potential cytotoxicity. The reduction in viability is likely due to mechanical trauma following removal of discs prior to the viability assay, as the discs were noted to stick slightly within the wells.

Further, cytocompatibility of conventionally electrospun 2D PBS-DLS membranes and 3D HCS was also evaluated by seeding L929 murine fibroblasts directly on samples of the materials (**Figure 8**). After 18 hours, the cell culture inserts holding the materials were transferred to fresh wells and cell viability was assessed using the resazurin assay—this value was considered to represent the adhesion of cells to the test materials. Next, cells were fed with fresh complete media and cell viability (Fig. 8a) was assessed after incubation for 48 hours, after which cells were again fed and viability was assessed after a further 96 hours (144 hours after transfer to fresh wells, 162 hours total) of culture—these values represent proliferation of cells on the materials. The initial adhesion on HCS (Fig. 8a) was observed to be lower, likely due to the loose, open morphology of the materials permitting cells to fall through, while the more compact nature of the flat 2D membranes acts as a filter. In fact, for HCS samples, after transferring all cell culture inserts to fresh wells, we observed marked viability signal from the well bottom. Importantly, after maintaining the scaffolds in culture, we observe higher viability of L929 cells on HCS, as compared to flat 2D mats (Fig. 6a,b) and the growth ratio (Fig. 8b), calculated per sample as the ratio of viability after each incubation

time to the initial value (after 18 hours), was significantly higher for HCS after both 48 hours (2.6 *vs.* 1.6, p = 0.02) and 144 hours (10.0 *vs.* 5.3, p = 0.01). We conclude that electrospun PBS-DLS materials are cytocompatible, based upon lack of cytotoxicity in extract and direct contact tests, as well as observed adhesion and growth of cells. Meanwhile, the marked increase in proliferation on HCS samples confirms the suitability of these 3D materials as scaffolds for soft tissue engineering.

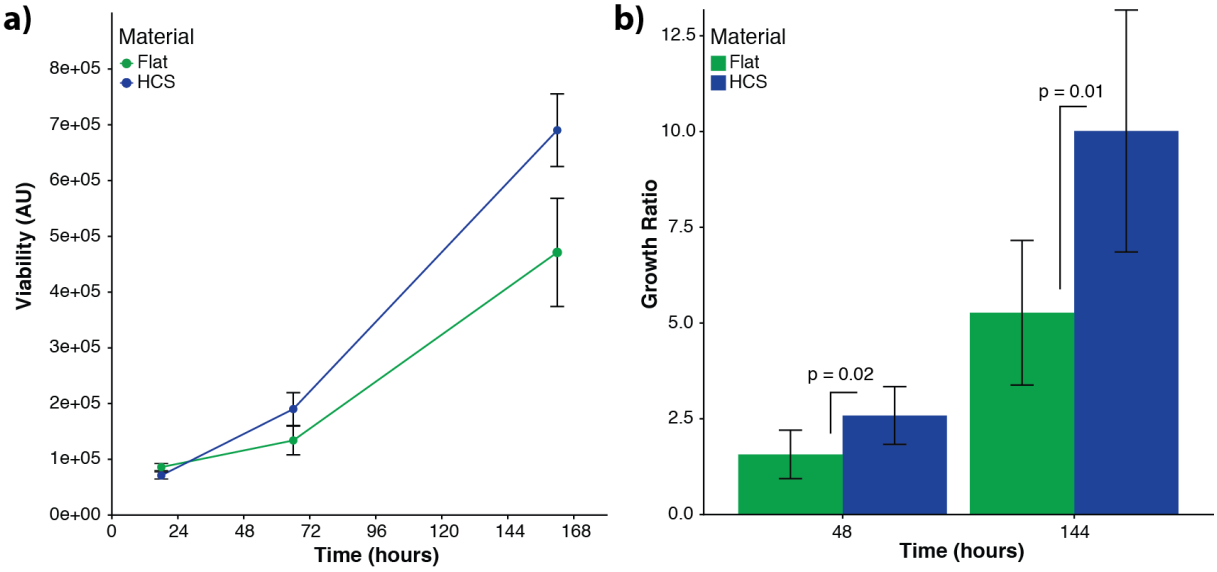

Figure 8. a) L929 cell viability (mean±SE) on conventionally electrospun 2D membranes (n=5) and HCS (n=10) 18 hours after seeding and following additional 48 hours and 144 hours of culture. b) Ratios (mean±SD) of viability after additional incubation time *versus* initial value after 18 hours, representing proliferation of L929 cells on test materials.

CONCLUSIONS

In conclusion, microscale helically coiled structures were fabricated by wet-electrospinning elastomeric poly(butylene succinate-co-dilinoleic succinate) copolymer with a 70:30 wt.% of hard to soft segments. Importantly, the fabricated 3D HCS have higher open porosity than conventionally spun 2D membranes. By tuning process parameters, PBS-DLS HCS could be obtained that mimic morphology of coiled fibers found in heart perimysium. Importantly, the mechanical properties of PBS-DLS HCS also closely resemble those of cardiac tissue. In terms of cytocompatibility, extract and direct contact cell culture tests did

not indicate cytotoxicity of electrospun PBS-DLS, while seeding cells on HCS resulted in ~2-fold higher proliferation than on conventionally spun 2D membranes. We conclude that the PBS-DLS HCS are well suited for applications in functional heart tissue engineering, as their elastomeric properties will help in cyclic contraction/retraction motion of the engineered cardiac tissue. Finally, our mechanics analysis indicates that HCS obtained *via* wet electrospinning are formed due to the combination of tensile and normal component of electric force acting on the electrospun jet, as well as the surface tension of the non-solvent bath. The discussed mechanism behind the formation of helically coiled structures in non-solvent bath may aid in the design and fabrication of HCS for functional tissue engineering, as well as various other applications.

AUTHOR INFORMATION

Corresponding Author

*E-mail: mirfray@zut.edu.pl.

ORCID

Miroslawa El Fray: 0000-0002-2474-3517

Author Contributions

The manuscript was written through contributions of all authors.

All authors have given approval to the final version of the manuscript.

Notes

The authors declare no competing financial interest.

ACKNOWLEDGEMENTS

This work is financially supported by National Science Centre, Poland, under the HARMONIA scheme (agreement No. UMO-2014/14/M/ST8/00610). The authors thank Dr. Karol Fijałkowski (Faculty of Biotechnology and Animal Husbandry, ZUT) for access to the multifunctional plate reader.

REFERENCES

(1) Sanchez, C.; Arribart, H.; Giraud Guille, M. M. Biomimetism and bioinspiration as tools for the design of innovative materials and systems. *Nat. Mater.* **2005**, *4* (4), 277–288 DOI: 10.1038/nmat1339.

(2) Jang, K. I.; Li, K.; Chung, H. U.; Xu, S.; Jung, H. N.; Yang, Y.; Kwak, J. W.; Jung, H. H.; Song, J.; Yang, C.; et al. Self-assembled three dimensional network designs for soft electronics. *Nat. Commun.* **2017**, *8*, 15894 DOI: 10.1038/ncomms15894.

(3) Saini, D.; Behlow, H.; Podila, R.; Dickel, D.; Pillai, B.; Skove, M. J.; Serkiz, S. M.; Rao, A. M. Mechanical resonances of helically coiled carbon nanowires. *Sci. Rep.* **2014**, *4*, 5542 DOI: 10.1038/srep05542.

(4) Hoshizawa, H.; Suzuki, M.; Shirai, H.; Hanabusa, K.; Yang, Y. Fabrication of Helical Mesoporous Silica Nanostructures Using Gelators and the Mixtures with CTAC. *Sen-I Gakkaishi* **2009**, *65* (2), 78–85 DOI: 10.2115/fiber.65.80.

(5) Giraldo, O.; Marquez, M.; Brock, S. L.; Suib, S. L.; Hillhouse, H.; Tsapatsis, M. Spontaneous formation of inorganic helical fibers and rings. *J. Am. Chem. Soc.* **2000**, *122* (49), 12158–12163 DOI: 10.1021/ja0018872.

(6) Lin, Y.; Qiao, Y.; Gao, C.; Tang, P.; Liu, Y.; Li, Z.; Yan, Y.; Huang, J. Tunable one-dimensional helical nanostructures: From supramolecular self-assemblies to silica nanomaterials. *Chem. Mater.* **2010**, *22* (24), 6711–6717 DOI: 10.1021/cm102181e.

(7) Kong, X. Y.; Wang, Z. L. Spontaneous Polarization-Induced Nanohelixes, Nanosprings, and Nanorings of Piezoelectric Nanobelts. *Nano Lett.* **2003**, *3* (12), 1625–1631 DOI: 10.1021/nl034463p.

(8) Zander, N. Hierarchically Structured Electrospun Fibers. *Polymers (Basel).* **2013**, *5* (1), 19–44 DOI: 10.3390/polym5010019.

(9) Lin, T.; Wang, H.; Wang, X. Self-crimping bicomponent nanofibers electrospun from polyacrylonitrile and elastomeric polyurethane. *Adv. Mater.* **2005**, *17* (22), 2699–2703 DOI: 10.1002/adma.200500901.

(10) Kessick, R.; Tepper, G. Microscale polymeric helical structures produced by electrospinning. *Appl. Phys. Lett.* **2004**, *84* (23), 4807–4809 DOI: 10.1063/1.1762704.

(11) Xin, Y.; Huang, Z. H.; Yan, E. Y.; Zhang, W.; Zhao, Q. Controlling poly(p-phenylene vinylene)/poly(vinyl pyrrolidone) composite nanofibers in different morphologies by electrospinning. *Appl. Phys. Lett.* **2006**, *89* (5), 53101 DOI: 10.1063/1.2236382.

(12) Shin, M. K.; Kim, S. I.; Kim, S. J. Controlled assembly of polymer nanofibers: From helical springs to fully extended. *Appl. Phys. Lett.* **2006**, *88* (22), 223109 DOI: 10.1063/1.2208689.

(13) Fleischer, S.; Feiner, R.; Shapira, A.; Ji, J.; Sui, X.; Daniel Wagner, H.; Dvir, T. Spring-like fibers for cardiac tissue engineering. *Biomaterials* **2013**, *34* (34), 8599–8606 DOI: 10.1016/j.biomaterials.2013.07.054.

(14) Butler, D. L.; Goldstein, S. A.; Guilak, F. Functional Tissue Engineering: The Role of Biomechanics. *J. Biomech. Eng.* **2000**, *122* (6), 570 DOI: 10.1115/1.1318906.

(15) Guilak, F.; Butler, D. L.; Goldstein, S. A.; Baaijens, F. P. T. Biomechanics and mechanobiology in functional tissue engineering. *J. Biomech.* **2014** DOI: 10.1016/j.jbiomech.2014.04.019.

(16) Robinson, T. F.; Geraci, M. a.; Sonnenblick, E. H.; Factor, S. M. Coiled perimysial fibers of papillary muscle in rat heart: morphology, distribution, and changes in configuration. *Circ. Res.* **1988**, *63* (3), 577–592 DOI: 10.1161/01.RES.63.3.577.

(17) Freed, L. E.; Engelmayr, G. C.; Borenstein, J. T.; Moutos, F. T.; Guilak, F. Advanced material strategies for tissue engineering scaffolds. *Adv. Mater.* **2009**, *21* (32–33), 3410–3418 DOI: 10.1002/adma.200900303.

(18) Jung, Y.; Park, M. S.; Lee, J. W.; Kim, Y. H.; Kim, S. H.; Kim, S. H. Cartilage regeneration with highly-elastic three-dimensional scaffolds prepared from biodegradable poly(l-lactide-co-ε-caprolactone). *Biomaterials* **2008**, *29* (35), 4630–4636 DOI: 10.1016/j.biomaterials.2008.08.031.

(19) Ki, C. S.; Kim, J. W.; Hyun, J. H.; Lee, K. H.; Hattori, M.; Rah, D. K.; Park, Y. H. Electrospun three-dimensional silk fibroin nanofibrous scaffold. *J. Appl. Polym. Sci.* **2007**, *106* (6), 3922–3928 DOI: 10.1002/app.26914.

(20) Yokoyama, Y.; Hattori, S.; Yoshikawa, C.; Yasuda, Y.; Koyama, H.; Takato, T.; Kobayashi, H. Novel wet electrospinning system for fabrication of spongiform nanofiber 3-dimensional fabric. *Mater. Lett.* **2009**, *63* (9–10), 754–756 DOI: 10.1016/J.MATLET.2008.12.042.

(21) Shin, T. J.; Park, S. Y.; Kim, H. J.; Lee, H. J.; Youk, J. H. Development of 3-D poly(trimethylenecarbonate-co-ε-caprolactone)-block-poly(p-dioxanone) scaffold for bone regeneration with high porosity using a wet electrospinning method. *Biotechnol. Lett.* **2010**, *32* (6), 877–882 DOI: 10.1007/s10529-010-0235-7.

(22) Hong, S.; Kim, G. Fabrication of size-controlled three-dimensional structures consisting of electrohydrodynamically produced polycaprolactone micro/nanofibers. *Appl. Phys. A* **2011**, *103* (4), 1009–1014 DOI: 10.1007/s00339-011-6381-5.

(23) Coburn, J. M.; Gibson, M.; Monagle, S.; Patterson, Z.; Elisseeff, J. H. Bioinspired nanofibers support chondrogenesis for articular cartilage repair. *Proc. Natl. Acad. Sci.* **2012**, *109* (25), 10012–10017 DOI: 10.1073/pnas.1121605109.

(24) Kasuga, T.; Obata, A.; Maeda, H.; Ota, Y.; Yao, X.; Oribe, K. Siloxane-poly(lactic acid)-vaterite composites with 3D cotton-like structure. *J. Mater. Sci. Mater. Med.* **2012**, *23* (10), 2349–2357 DOI: 10.1007/s10856-012-4607-5.

(25) Gang, E. H.; Ki, C. S.; Kim, J. W.; Lee, J.; Cha, B. G.; Lee, K. H.; Park, Y. H. Highly porous three-dimensional poly(lactide-co-glycolide) (PLGA) microfibrous scaffold prepared by electrospinning method: A comparison study with other PLGA type scaffolds on its biological evaluation. *Fibers Polym.* **2012**, *13* (6), 685–691 DOI: 10.1007/s12221-012-0685-8.

(26) Kim, M. S.; Son, J.; Lee, H.; Hwang, H.; Choi, C. H.; Kim, G. Highly porous 3D nanofibrous scaffolds processed with an electrospinning/laser process. *Curr. Appl. Phys.* **2014**, *14* (1), 1–7 DOI: 10.1016/J.CAP.2013.10.008.

(27) Kim, M. S.; Kim, G. Electrohydrodynamic Jet Process for Pore-Structure-Controlled 3D Fibrous Architecture As a Tissue Regenerative Material: Fabrication and Cellular Activities. *Langmuir* **2014**, *30* (28), 8551–8557 DOI: 10.1021/la501080c.

(28) Kostakova, E.; Seps, M.; Pokorny, P.; Lukas, D. Study of polycaprolactone wet electrospinning process. *Express Polym. Lett.* **2014**, *8* (8), 554–564 DOI: 10.3144/expresspolymlett.2014.59.

(29) Díez-Pascual, A. M.; Díez-Vicente, A. L. Electrospun fibers of chitosan-grafted polycaprolactone/poly(3-hydroxybutyrate-co-3-hydroxyhexanoate) blends. *J. Mater.*

Chem. B **2016**, *4* (4), 600–612 DOI: 10.1039/C5TB01861G.

(30) Colpankan Gunes, O.; Unalan, I.; Cecen, B.; Ziylan Albayrak, A.; Havitcioglu, H.; Ustun, O.; Ergur, B. U. Three-dimensional silk impregnated HAp/PHBV nanofibrous scaffolds for bone regeneration. *Int. J. Polym. Mater. Polym. Biomater.* **2018**, 1–12 DOI: 10.1080/00914037.2018.1443928.

(31) Taskin, M. B.; Xu, R.; Gregersen, H.; Nygaard, J. V.; Besenbacher, F.; Chen, M. Three-Dimensional Polydopamine Functionalized Coiled Microfibrous Scaffolds Enhance Human Mesenchymal Stem Cells Colonization and Mild Myofibroblastic Differentiation. *ACS Appl. Mater. Interfaces* **2016**, *8* (25), 15864–15873 DOI: 10.1021/acsami.6b02994.

(32) Sonseca, A.; El Fray, M. Enzymatic synthesis of an electrospinnable poly(butylene succinate-co-dilinoleic succinate) thermoplastic elastomer. *RSC Adv.* **2017**, *7* (34), 21258–21267 DOI: 10.1039/C7RA02509B.

(33) Liverani, L.; Piegat, A.; Niemczyk, A.; El Fray, M.; Boccaccini, A. R. Electrospun fibers of poly(butylene succinate–co–dilinoleic succinate) and its blend with poly(glycerol sebacate) for soft tissue engineering applications. *Eur. Polym. J.* **2016**, *81*, 295–306 DOI: 10.1016/j.eurpolymj.2016.06.009.

(34) Jäger, A.; Gromadzki, D.; Jäger, E.; Giacomelli, F. C.; Kozlowska, A.; Kobera, L.; Brus, J.; Říhová, B.; El Fray, M.; Ulbrich, K.; et al. Novel "soft" biodegradable nanoparticles prepared from aliphatic based monomers as a potential drug delivery system. *Soft Matter*. 2012, p 4343.

(35) Kozłowska, A.; Gromadzki, D.; El Fray, M.; Štêpánek, P. Morphology evaluation of biodegradable copolyesters based on dimerized fatty acid studied by DSC, SAXS and WAXS. *Fibres Text East Eur* **2008**, *16*, 85.

(36) ISO. *Biological evaluation of medical devices—Part 5: tests for in vitro cytotoxicity*; Geneva, Switzerland, 2009.

(37) Riss, T. L.; Moravec, R. A.; Niles, A. L.; Duellman, S.; Benink, H. A.; Worzella, T. J.; Minor, L. Cell Viability Assays. In *Assay Guidance Manual*; Sittampalam, G., Coussens, N., Eds.; Eli Lilly & Company and the National Center for Advancing Translational Sciences: Bethesda, MD, 2004.

(38) Spinks, G. M. Stretchable artificial muscles from coiled polymer fibers. *J. Mater. Res.* **2016**, *31* (19), 2917–2927 DOI: 10.1557/jmr.2016.316.

(39) Ross, A. L. Cable Kinking Analysis and Prevention. *J. Eng. Ind.* **1977**, *99* (February), 112 DOI: 10.1115/1.3439123.

(40) Feng, J. J. The stretching of an electrified non-Newtonian jet: A model for electrospinning. *Phys. Fluids* **2002**, *14* (11), 3912–3926 DOI: 10.1063/1.1510664.

(41) Reneker, D. H.; Yarin, A. L. Electrospinning jets and polymer nanofibers. *Polymer (Guildf).* **2008**, *49* (10), 2387–2425 DOI: 10.1016/j.polymer.2008.02.002.

(42) Neukirch, S.; Roman, B.; de Gaudemaris, B.; Bico, J. Piercing a liquid surface with an elastic rod: Buckling under capillary forces. *J. Mech. Phys. Solids* **2007**, *55* (6), 1212–1235 DOI: 10.1016/j.jmps.2006.11.009.

(43) Roman, B.; Bico, J. Elasto-capillarity: Deforming an elastic structure with a liquid droplet. *J. Phys. Condens. Matter* **2010**, *22* (49), 493101 DOI: 10.1088/0953-8984/22/49/493101.

(44) Huang, J.; Juszkiewicz, M.; De Jeu, W. H.; Cerda, E.; Emrick, T.; Menon, N.; Russell,

T. P. Capillary wrinkling of floating thin polymer films. *Science (80-.).* **2007**, *317* (5838), 650–653 DOI: 10.1126/science.1144616.

(45) Lim, J. Y.; Donahue, H. J. Cell Sensing and Response to Micro- and Nanostructured Surfaces Produced by Chemical and Topographic Patterning. *Tissue Eng.* **2007**, *13* (8), 1879–1891 DOI: 10.1089/ten.2006.0154.

(46) Chen, Q.-Z.; Bismarck, A.; Hansen, U.; Junaid, S.; Tran, M. Q.; Harding, S. E.; Ali, N. N.; Boccaccini, A. R. Characterisation of a soft elastomer poly(glycerol sebacate) designed to match the mechanical properties of myocardial tissue. *Biomaterials* **2008**, *29* (1), 47–57 DOI: 10.1016/j.biomaterials.2007.09.010.